Computational Geosciences manuscript No.
(will be inserted by the editor)

On Obtaining Optimal Well Rates and Placement for CO_2 Storage

Rebecca Allen · Halvor Møll Nilsen · Odd Andersen · Knut-Andreas Lie

Received: date / Accepted: date

Abstract Large-scale storage of CO_2 in saline aquifers is considered an essential technology to mitigate CO_2 emissions. Storage potential has mainly been estimated based on volumetrics or detailed simulations for specific injection scenarios. In practice, achievable storage capacity will depend on engineering, economical, and political restrictions and be limited by the length of the injection period, costs associated with potential CO_2 leakage, pressure management, etc.

We show how achievable storage volumes can be estimated and maximized using adjoint-based optimization and a hierarchy of simulation methods. In particular, vertical equilibrium models provide the simplest possible description of the flow dynamics during the injection and early post-injection period, while percolation type methods provide effective means for forecasting the long-term fate of CO_2 during the later migration stages.

We investigate the storage volumes that can be achieved for several formations found along the Norwegian Continental Shelf by optimizing well placement and injection rates, and using production wells for pressure management when necessary. Optimal strategies are obtained under various objectives and simple but realistic constraints, namely: penalization of CO_2 leakage, minimization of well cost, and restriction of pressure buildup.

Keywords Geological CO_2 storage · Large-scale injection · Vertical equilibrium simulations · Dynamic storage estimates · Optimization · Pressure management · Forecast leakage

Rebecca Allen
E-mail: Rebecca.Allen@sintef.no

Halvor Møll Nilsen
E-mail: HalvorMoll.Nilsen@sintef.no

Odd Andersen
E-mail: Odd.Andersen@sintef.no

Knut-Andreas Lie
E-mail: Knut-Andreas.Lie@sintef.no

SINTEF Digital, Mathematics and Cybernetics
P.O. Box 124 Blindern, N–0314 Oslo, Norway

1 Introduction

There is scientific consensus that anthropogenic CO_2 emission cause climate changes which threaten the economical and political stability of the world. The development of our modern world has been largely driven by an ever-increasing energy consumption. Today, 80% of the world's energy is based on fossil fuel [25]. To enable a transition to a society based on energy resources with no CO_2 emission in a time frame that prevents severe consequences in terms of climate change and need for substantial socioeconomic changes, it is believed that large-scale capture and storage of CO_2 in saline aquifers is needed (see summary for policymakers in the IPCC report [43]). Indeed IPCC states with high confidence that: "*Many models could not limit likely warming to below 2° C if bioenergy, CCS and their combination (BECCS) are limited*". In their overview of mitigation cost, limitation of available BECCS and CCS are dominating.

After 20 years of research there are less than 40 pilot projects with CO_2 injection in the world, and all of them are small compared with the scales needed for CO_2 storage to be a viable mitigation strategy. Although a large research effort has focused on storage capacity estimates and simulation strategies, little work has been devoted to developing general workflows and

methods for aquifer-wide estimates. Many regional and world-wide estimates use simple volumetrics [44,3,5,23,7], but such estimates are difficult to use reliably because of wide variation in geological properties [9]. As discussed in a recent review by Bachu [2], local storage potential should be estimated using site-specific calculations to be able to account for all the factors important for storage. In addition to this, there are several site-specific simulation studies [48,16,19,17,49], benchmark comparisons [13,42], or demonstration of new methods for CO_2-specific simulation methods [20,32,11]. Presently, more and more surveys are aimed at providing detailed storage capacity estimates for large-scale regions containing plausible storage sites [29,8,15,23,35,47,14]. Until more detailed models that include all the major aspects that decide the storage potential become widely available (including aquifer characteristics, operational constraints, regulatory constraints and economical constraints [2]), we believe that integrated frameworks that combine a variety of different computational and optimization methods will be a key technology for estimating storage capacities, devising plans, and determining the economical feasibility of large-scale injection projects.

In previous work we have developed a toolchain of methods integrated into an open-source framework [33] with a specific CO_2 module [34]. The methods range from simple geometrical estimates [39], via vertical equilibrium (VE) simulations [37,38], to 3D simulation tools for general grids [30,28]. The advantage of such a toolchain was demonstrated by combining different methods in a workflow [1] to make dynamic estimates for storage potential under simplified assumptions for formations from the CO_2 Storage Atlas of the Norwegian Continental Shelf [23]. Furthermore, more accurate storage estimates and use of mathematical optimization were demonstrated by Nilsen et al. [36,40]. Herein, we will enhance our chain of methods with capabilities to handle pressure constraints and more realistic economical constraints. Pressure limitations for large-scale CO_2 injection have received more attention in recent years, e.g., as discussed in the recent review by Birkholzer et al. [6]. Our new methods are applied to a series of test cases where the storage capacity that can be practically achieved is limited by leakage during injection, pressure buildup due to injectivity, and cost of drilling and operating injection wells. For formations with open boundaries, we present a new and approximate optimization method for storage volumes which significantly reduces the computational cost of forward simulations by combining VE simulation (for the injection and early migration period) with a forecast algorithm (for the later migration period) to determine the long-term fate of the free CO_2 plume. The forecast algorithm is based on spill-point analysis and calculation of catchment areas.

Forecasts of likely outcomes and proposed injection plans are obviously no better than the input data used to generate them. In particular, variation in geological structures and rock properties is a huge source of uncertainty in flow modeling both on small-scale, reservoir-scale, and basin-scale. Even for reservoirs that are well characterized, this uncertainty dominates the predictive power of flow models. On basin-scale, and in particular for saline aquifers where the economical advantages of detailed characterization are not immediately evident, the model uncertainties are even larger. This lack of detailed characterization is reflected in the aquifer models in the CO_2 Storage Atlas from the Norwegian Petroleum Directorate (NPD) [23]. In the public data sets, permeabilities and porosities are uniform and there is no fault information. There is also no information about spatially varying thermal gradients or possible leakage through the caprock. We acknowledge that these are important factors, but in spite of these limitations we have decided to use these openly available data to demonstrate our modeling framework and discuss its advantages and potential benefits in future CCS operations. We emphasize that our framework is very flexible and easily extensible; our computational methods rely on cell-based quantities and can therefore be used on heterogeneous basin-scale models like in [32], if and when such models become generally available. Moreover, our methods are based on general gridding so that complex geometry can easily be incorporated, for example to model faults. Caprock leakage can also be included with trivial modifications of the methods.

2 Simulation Methods

When CO_2 is injected deep into a saline aquifer, the main dynamics is governed by different physical processes in time and space. Thus, different modeling choices and methods are preferable at different stages of the injection and migration process. In the initial phase, the flow is viscous dominated near the well and in general in the whole formation. Moving farther away from the well, gravity becomes a more dominant force, and even when other forces are stronger, the long-term effect of gravity will lead to a gradual segregation. Near the well, 3D flow dynamics and detailed pressure evolution including thermal and mechanical effects is important and in many cases, modified versions of 3D simulation tools developed for reservoir simulation will be the right choice. Later in the injection phase, much of the CO_2 will be found under a ceiling caprock in a relatively thin layer at a larger distance from the well. In this part,

gravity and capillary forces are in vertical equilibrium in layers with good communication, and viscous forces due to pressure gradients dominate the flow. If 3D simulation is used, care has to be taken both in defining the vertical resolution and relative permeabilities to accurately resolve sharp interfaces and thin layers. Small time steps may also be necessary to capture the coupling between pressure and transport of phases in the vertical direction. VE methods often have a greater advantage for this dynamics, in particular in combination with sequential simulation strategies that split the dynamics of pressure and transport of fluid phases.

When injection stops, the system will change dramatically. Near the injection well there will no longer be a strong pressure gradient. However, there is a pressure gradient in the plume, and initially the dynamical effect is a redistribution of pressure, which results in an expansion of the CO_2 plume. The latter will cause the fluid interface between the plume and the resident brine to gradually become flatter, which seen as a 3D process, is an effect due to rotational velocity fields enforced by the angle between the fluid interface and gravity. This process is driven by a coupling of transport and pressure. In a 2D VE model, this process is mainly seen in the transport equation as a parabolic (diffusion) process that smooths the CO_2 interface towards a horizontal position, and the coupling of transport and pressure is weaker because of the vertical integration.

Far from the well and in the late post-injection period, which typically takes place more than 100 years after injection has ceased, buoyancy forces will completely dominate and be in equilibrium with capillary pressure in the vertical direction. If the CO_2 plume is thin, which it typically will be outside of traps, the CO_2 will move in the upslope direction. In this case, a topographical analysis, similar to a watershed analysis in water modeling or ray-tracing methods used to model oil migration in basin modeling, will give a good description of the future dynamics of the movable CO_2. This effect is a coupling between pressure and transport in the 3D model, while in the 2D VE model it is a hyperbolic transport mechanism and hence can be computed more efficiently. When the CO_2 plume has considerable thickness—which is typical for all CO_2 just after injection, for CO_2 flowing upward along 'ridges' in the caprock, and in regions with geometrical traps which are relatively flat—the coupling between viscous forces and gravity pressure is important for the CO_2 movement. For most of this dynamics, a VE type model discretized with a fully-implicit method will be the preferable choice to capture the delicate balance of forces; see the discussion in e.g., Nilsen et al. [38].

Some of the injected CO_2 will also dissolve in the resident brine. Dissolution retards and limits the extent of the plume migration and can increase storage capacity by a factor of two or more compared to what is attainable by structural trapping alone and is therefore important to include in VE models, as discussed e.g., in [38]. Brine with dissolved CO_2 is heavier than pure brine and will sink to the bottom, forming gravity-driven instabilities that may in turn significantly enhance the dissolution rate, depending upon the heterogeneity of the formation [18]. This convective mixing is difficult to compute, and although its effect is widely discussed, it is hard to find good data for real cases, see [38]. When CO_2 dissolves in brine, it forms a weak carbonic acid, which can react with minerals in the surrounding rock and form carbonate minerals that trap the CO_2. Solubility and mineral trapping are the most stable trapping mechanisms and will generally contribute to increase storage capacity beyond what is estimated by studying structural and residual trapping, as we will do herein.

We start our description of methods by discussing the topographical analysis used to determine structural traps in the caprock and forecast the late, large-scale evolution of the CO_2 plume. Then, we briefly describe the more detailed VE simulation methods used for the earlier phase of the storage process, before we describe how the two can be combined to efficiently forecast the long-term fate of injected CO_2.

2.1 Topographical analysis

During the migration phase, buoyancy is the dominant driving force for CO_2 migration. This is analogous to primary migration of hydrocarbons or large-scale water flow in watersheds and rivers. It has been shown that simulations using traditional Darcy-type simulation can lead to large errors [46], in particular in 3D models that lack sufficient spatial resolution. Unless CO_2 is found in a large plume, which mainly happens in traps, the dynamics has many similarities to primary migration, even though the time-scales are much shorter and the rates much higher for CO_2 migration than for oil and gas migration. Grover et al. [22] describe how a code developed for simulating primary hydrocarbon migration was adapted to model CO_2 migration, and estimates of CO_2 storage computed for the Trøndelag platform are presented by Lothe et al. [32]. Their approach is very similar to the approach we use herein, which was presented in detail by Nilsen et al. [39] as a fast method for obtaining simple and preliminary estimates of CO_2 migration that later should be refined by more comprehensive dynamic simulations.

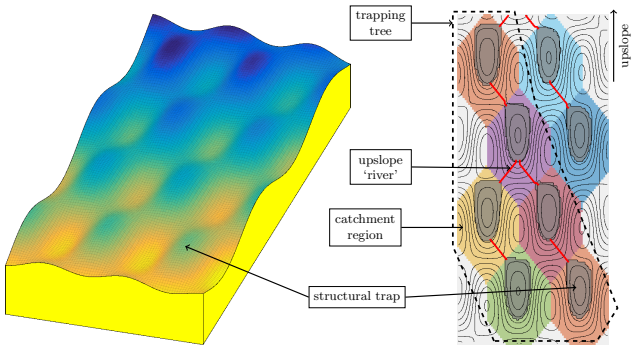

Fig. 1 Illustration of a topographical analysis of a sloping aquifer.

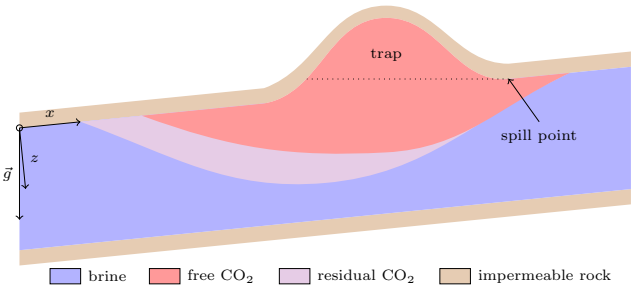

Fig. 2 Illustration of a sharp-interface VE model with residual and structural trapping.

The main component of all of these methods is that CO_2 moves upwards driven by buoyancy forces. Primary-migration codes use ray-tracing, which also includes loss mechanisms along rays, while we base our method purely on a discrete representation of the caprock topography. The result in both cases is that CO_2 flows upwards to the nearest trap, which will be gradually filled until it overflows. The CO_2 will then continue to migrate upward, in analog to how water flows from a watershed and into the nearest pond, brook, lake or river and then either stops or continues to flow downwards towards the sea level. From an algorithmic point of view, these methods are also connected to image segmentation techniques; see Roerdink and Meijster [45]. For the calculations in this paper we use topographical information describing the traps, their connection, and their storage capacity, which can be obtained by relatively simple geometrical and topological analysis of the surface grid representing the interface between the aquifer and the overlying caprock. This analysis will also give us information of the catchment area (inflow region) of each trap or aquifer perimeter. This is illustrated in Figure 1. The resulting trap structure can be described as a directed graph that consists of a set of trees. Using this information, we can forecast the eventual fate of free CO_2 located at any map position in the aquifer. Assuming that structural trapping is the only trapping mechanism, the free CO_2 will either migrate into one of the traps found upslope of the point and be confined there, or reach the model perimeter if the point is part of its catchment area or if all upslope traps are already filled.

2.2 Vertical equilibrium (VE) models

A typical saline aquifer can span thousands of square kilometers but will seldom have a thickness that exceeds tens or a few hundred meters. Because of the density difference between resident brine and the injected (supercritical) CO_2 and the long time-scales of a typical simulation period (thousands of years), the vertical fluid segregation will be almost instantaneous compared with the upslope migration of the plume. For most of the simulation, CO_2 will therefore be confined to thin layers underneath the sealing caprock or other low-permeable vertical barriers (the exception is the near-well region and traps with a significant height). The large disparity in lateral and vertical scales means that the aquifer system can be considered as a relatively thin sheet, with another and thinner CO_2 sheet inside that drapes parts of the caprock from below. Capturing the vertical fluid distribution will in most cases require a much higher vertical resolution than what is computationally tractable for 3D simulation, and such simulations therefore tend to be severely under-resolved.

Using a VE assumption, the flow of a (thin) CO_2 plume is approximated in terms of its thickness to obtain a reduced model. To this end, vertical integration is first used to reduce the spatial dimensions of the model from 3D to 2D. Then we impose an assumption of vertical equilibrium in the form of an analytic model that can be used to determine the vertical fluid distribution. In its simplest form, this model describes a sharp interface that separates pure CO_2 on top from brine at the bottom of the aquifer. This model can be extended to include pseudo-phases (or states) consisting of brine with residually trapped CO_2, brine with dissolved CO_2, and so on (see Figure 2). Using these pseudo-phases, it is simple to develop detailed inventories that report to what extent CO_2 has been trapped by different trapping mechanisms and to what extent it is free to move about (see Figure 3). In more advanced models, the interface between CO_2 and brine consists of a capillary fringe that is determined by the fine-scale capillary pressure.

The flow equations of VE models can be written in the same form and discretized using the same methods as for conventional Darcy-type models. The only difference is how to interpret the primary variables and the fact that the vertical integration introduces pres-

sure dependence and hysteretic effects in some of the effective parameters. Note also that important information about the heterogeneities in the underlying 3D medium is preserved in an averaged sense through upscaled effective properties that depend on the particular assumption used to model the vertical fluid distribution. Integration in the vertical direction not only reduces the number of spatial dimensions, and hence the required number of grid cells, but will also lessen the coupling between pressure and fluid transport and hence improve the characteristic time constants of the problem. As a result, VE simulators will typically be orders of magnitude faster and consume significantly less memory than conventional 3D simulators. For a more thorough discussion of the exact formulations we use in our open-source framework (MRST), and an overview of previous work on VE models, we refer the reader to Nilsen et al. [38,37].

2.3 Forecasting long-term leakage

Defining the amount of CO_2 that should be considered to be permanently stored is a complex political and regulatory question. Obviously, there is no 100% guarantee that CO_2 existing in a movable state cannot at some point leak back to the earth surface or sea floor. Herein, we will consider all amounts of CO_2 that are confined within structural traps as permanently stored, and likewise for CO_2 that is residually trapped, dissolved into brine, or minerally trapped. (For simplicity, the latter two to three mechanisms will be neglected in our examples later in the paper.)

This leaves us with the question of the part of the CO_2 found outside of structural traps which is free to move around. What amount of CO_2 should be considered likely to leak will obviously depend on the regulatory and legislative framework, insurance policies, agreements between operators working in different acreages within the same aquifer systems, etc. Should we only care about volumes leaving a predefined area within the next 100 years, the next 1000 years, or the next million years? Herein, we will make a somewhat simplistic choice. We assume that there will be no geological activity to change the aquifer and consider the amount of CO_2 that has migrated across open aquifer boundaries during the simulation period as leaked. To avoid having to simulate the migration for a very long period, we will also use a simplified and conservative forecast method as illustrated in Figure 3. If we disregard the effect of residual and solubility trapping, a simple spill-point and trapping analysis can be used to forecast where the CO_2 will migrate to at time infinity. Any CO_2 volume that is not within the catchment area of a structural trap is destined to eventually migrate to the aquifer boundary, and if these are open, the volumes will leak. Any volume that is found within a catchment region of a trap will eventually migrate into this trap and be confined there, unless the migrating volume is so large that the trap over flows. The excess volume will then continue to migrate upward and either fill another trap or reach the aquifer boundary.

3 Optimization Methods for Maximal Utilization

In this section, we describe various heuristic and more mathematically rigorous workflows that can be used to devise plausible plans for maximal utilization of trapping capacities. These methods are extensions of methods that have already been presented by Nilsen et al. [39, 36] and Lie et al. [31]. Our aim is to exploit as much of the formation's storage capacity as possible. In the following, we will therefore tacitly assume that structural traps can and have been identified, as well as their catchment areas, and the spill-paths that connect several traps along a spill-tree. The cumulative structural capacity of a spill-tree can also be calculated, so that we can see the reachable structural capacity for each point within a given catchment area.

3.1 Optimization framework

The simplest objective function imaginable for an open aquifer system would simply measure the amount of CO_2 injected and penalize the amount of CO_2 that has left the aquifer through the open boundaries or by leakage through the caprock. This can be expressed as

$$J = M_i - CM_l, \tag{1}$$

where M_i is mass injected, M_l is mass leaked, and C is the penalization factor. As discussed above, there are many ways to define the amount that has leaked. Herein, we will either use the amount that has migrated across the open aquifer boundaries during the simulation period or our simplified and conservative forecast of future leakage, i.e., the amounts that are destined to eventually migrate across open aquifer boundaries. This latter definition deviates from the objective function used in our previous work [31].

At the maximum of (1), we know that $0 < M_l < M_i/C$. For example, if regulations required leakage to be less than 5 percent of the total amount injected, one would use a leakage penalty factor of $C = 20$. Whether the leakage should be part of the objective function or

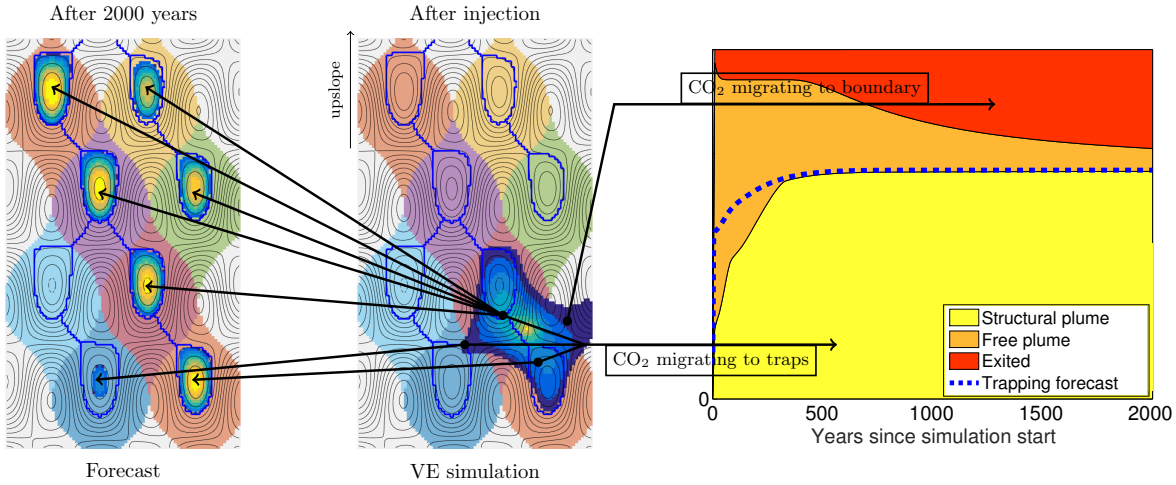

Fig. 3 Illustration of our procedure used to forecast volumes of CO_2 that eventually will leak as a result of migration. Using the catchment areas resulting from a trapping and spill-point analysis, we delineate the CO_2 plume into volumes that are destined to migrate to the aquifer boundary and volumes that will migrate up into a succession of shallower traps. If the latter volume is larger than the overall volume of the upslope traps, the excess volume is also destined to migrate to the aquifer boundary. The right plot shows an inventory of carbon trapping, where the trapped volumes are presented as function of time. The volumes are stacked and colored according to increasing risk of leakage: yellow for volumes that are confined inside a structural trap, orange for the movable plume, red for volumes that have leaked across the aquifer boundaries. (If residual and solubility trapping were included, these would have been colored in various shades of green, implying that they are more permanent.) The dashed blue line shows trapped volume at time infinity estimated if we start the forecast from the computed CO_2 distribution at this instance in time. (The curve is generated by performing a new forecast at the end of each time step in the VE simulation.) Note that pressure-driven flow will cause CO_2 to swell and spill into the green catchment region, consequently filling the two upper right traps; we discuss this further in Section 4.2.

imposed as a constraint will depend on whether the regulatory framework allows such leakage or not. Notice, in particular, that using (1) with a high constant C would be an approximation to the case of no leakage, $C \to \infty$. As for all methods relying on penalization, we have to be careful with high penalization since this introduces steep slopes in the objective function which may significantly reduce the efficiency of the optimization procedure.

Pressure buildup will likely be the limiting factor for how much CO_2 can be safely injected into a closed aquifer system. However, the integrity of the caprock is still of concern in open aquifer systems, and could limit the rate of injection. Thus for either type of aquifer systems, it is natural to consider penalization of pressure

$$J_p = J - C_p \sum_i \left(\max(0, p_i - p_i^{\max})\right)^2, \tag{2}$$

where C_p is the pressure penalization factor, p_i and $p_i^{\max}$ are the cell's pressure and predefined pressure limit respectively, and where the sum runs over all cells in the simulation model. Cell pressure is penalized only when it surpasses its limit, and its penalization grows quadratically the further it surpasses its limit. In this case, we use an optimization strategy in which the value of C_p is gradually ramped up as the iterations of the optimization scheme progress.

One important question here, given the lateral extent of grid cells which is typically from $\mathcal{O}(10^{-1})$ to $\mathcal{O}(10^{1})$ km in most large-scale aquifer models, is whether the computed cell pressures will represent the maximum pressure exerted on the caprock. For a vertical well completed throughout most of the aquifer height, the cell pressure will obviously underestimate the maximal pressure near the wellbore. However, a more likely injection scenario would be to place a long horizontal well near the bottom of the aquifer to maximize residual trapping and enable the plume to spread out more before its upward movement becomes limited by the caprock topography. In this case, the cell pressures in the VE model are a reasonable approximation.

The two simple formulations above have the obvious disadvantage that there is no cost associated with the drilling and operation of each well and hence it is highly plausible to find optimal injection scenarios that have (far too) many wells. Likewise, our objective does not take into account any economic incentives or deterrents. Since industry is liable to pay a tax on every tonne of CO_2 they emit, the amount of CO_2 that is injected and stored rather than emitted can be converted into a monetary value. The amount of money saved by injecting CO_2 is the worth of the stored CO_2 mi-

nus the project costs (i.e., acquiring CO_2, drilling and operating the wells). The objective function will then conceptually be of the form

$$J_v = (M_i - CM_l)R^{tax} - \sum_w \Big(C_w^{inv} + R_w^{op} M_{i,w}\Big) I_w, \quad (3)$$

where R^{tax} is CO_2 tax credit, C_w^{inv} is the investment cost to drill one well, R_w^{op} is the operational cost to acquire and inject CO_2, and I_w is an indicator function that is one if the well is present and zero otherwise. One can also easily imagine more comprehensive objective functions that e.g., account for cost of monitoring solutions, etc. Unfortunately, the introduction of an investment cost if a well is present turns the optimization problem into a mixed-integer problem. Regularizing I_w would be an obvious choice, but this may introduce multiple maxima, including one corresponding to zero rate, and the optimization algorithm will easily be stuck in a local optimum. A simple brute-force procedure would be to pick a number of wells and optimize, pick another combination of wells and optimize, compare the two, and so on. A general and efficient treatment of this problem is outside the scope of this paper.

3.2 Well placement

In principle, the above objective functions can be used to both determine the optimal number and placement of wells. This joint optimization, however, is a hard problem. In reservoir simulation the control optimization has often used gradient based techniques while well placement often is based on derivative-free algorithms or stochastic search procedures [4]. The basic parameter space of the well placement is large, even for a single well, and since the space is multiplicative with the number of wells, the complexity grows quite rapidly. In addition for a given grid model which in a geological setting often has finite resolution and is discrete, gradients are difficult to define. In this work we will therefore only consider fixed well positions. Three possible well placement strategies are:

1. Wells are placed in a uniform mesh covering the catchment areas of the formation. Whether a well is placed at a mesh node is subject to a buffer constraint that keeps the wells a certain distance from the aquifer perimeter and a density constraint that says that at most 30 percent of the cells in a catchment area can contain a well. This placement scheme may give a difficult optimization problem but is a general formulation that could be used for well placement optimization, e.g., start by placing many pseudo wells and only activate those that contribute most in maximizing the objective function under the given constraints.
2. One well per catchment area, placed at the highest elevation point or furthest downslope, as long as buffer constraints are satisfied. The injection mass per well is calculated based on the capacity of the associated trap. This approach is aimed at giving as much as possible of geometrical trapping with injection wells positioned to limit the chance for interaction between the injected plumes.
3. Wells placed using a simple *greedy* approach, as explained in [39,31], where wells are placed one by one in the deepest leaf nodes of the spill-tree with the greatest available reachable capacity. The well rate is computed based on the capacity along the spill-path connected to the leaf node. In the deepest leaf node, the well is placed as far downslope as possible (while maintaining a predefined buffer distance to the perimeter) to exploit as much residual trapping as possible.

There will generally be a maximum number of wells that can be placed. If we disregard well costs, the user can prescribe a maximum number of wells, and then the algorithms will continue to add wells until the assigned well rates fully exploit the structural trapping capacity of the formation or until the last well placed is assigned a well rate that is e.g., less than 1 percent of the first well rate. More realistically, one could impose the condition that each well should be able to cover its own investment and operational costs. That is, each well must inject a critical mass,

$$M_{crit} = C^{inv}/(R^{tax} - R^{op}), \quad (4)$$

that remains in the formation within the required time span. Hence, we terminate the placement of new wells if the next well to be added is not connected upslope to a sufficiently large volume. Figure 4 illustrates these well placement approaches applied to the Tubåen formation.

3.3 Finding an optimum

Once an objective function and set of injection points have been chosen, we can start to determine what will be the best injection strategy subject to engineering, economic, and regulatory constraints. The most basic task is to find what we will refer to as the dynamic storage capacity, i.e., optimize (via simulation) the amount of stored CO_2 constrained by the amount of fluids allowed to leave an open aquifer system, or by the pressure at the top of the formation. In most of our work, these constraints will be handled by penalization of the

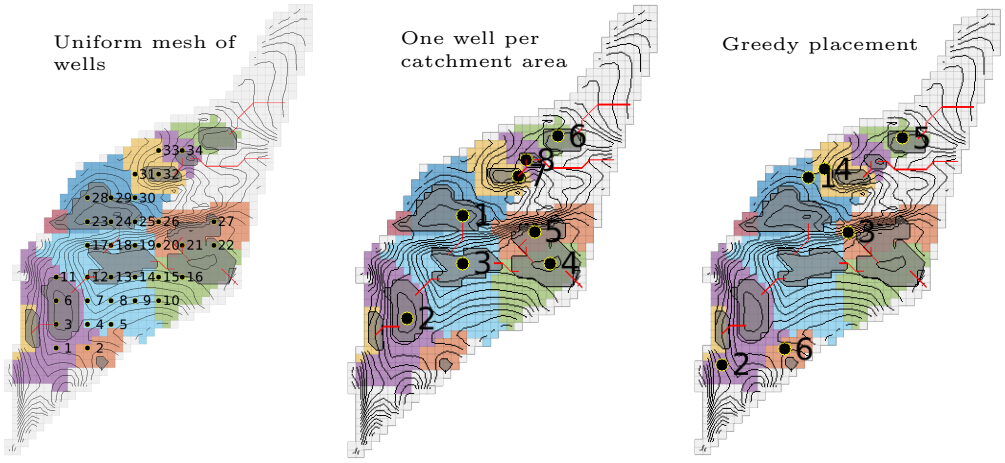

Fig. 4 Three possible well placement approaches applied to Tubåen, a formation located in the Barents Sea [23].

given quantity. We also consider using constraints directly on linear combinations of control variable in well pressure. In future work we will investigate further what is the right solution strategy for the constraints. Possible alternatives to our penalty method are interior-point, barrier, or augmented Lagrangian methods [12]. However, in this paper we use variants of the penalization method. In cases where we seek to minimize or avoid leakage, we treat the problem by including a constant penalization representing the cost of leakage, while for overburden pressure we use stepwise increasing penalization to approximate the constraint.

For the optimization, we use the Broyden–Fletcher–Goldfarb–Shanno (BFGS) algorithm, which is a quasi-Newton method, using the Wolfe conditions [50,51] with an inexact cubic line-search based on values and derivatives. The algorithm handles equality and inequality constraints by projection. In our problem, inequality constraints are used to enforce well rates to be non-negative while remaining within some absolute upper bound. The objective function will in our case depend on state variables that are obtained from a simulation which is determined by the unknown control variables to be optimized. We use the adjoint method for calculating derivatives with respect to these variables; see Jansen [27] and Hou et al. [24] for a review related to reservoir modeling. The advantage of this method compared with pure numerical derivatives is that one gets exact derivatives of the numerical objective function and that it is more efficient for a large number of control variables.

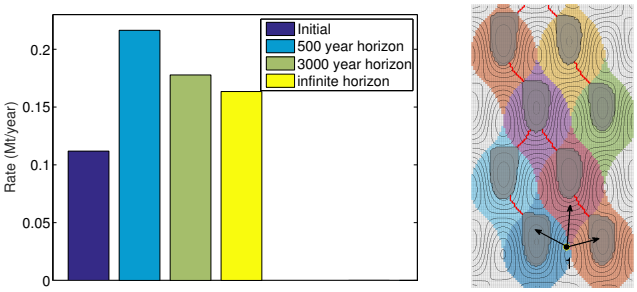

Fig. 5 Rate optimization for a single injection well in a conceptual aquifer model.

4 Maximizing Utilization of Structural Capacity

In this section, we will assume that we have an open aquifer system and use the simple objection function (1) to maximize the utilization of structural trapping capacity. We first consider a conceptual model to illuminate the basic principles, and then apply the same optimization method to the northern parts of the Utsira formation. We have not included injectivity of a single wellbore as a hard constraint in our optimization. This means that well rates will only be limited by storage capacity and pressure buildup, and in several cases, we end up with rates that are higher than what is likely realistic for a single wellbore. In the following, the word 'well' is really referring to injection points or injector hubs that may contain several individual injector wells.

4.1 Conceptual model

We first consider optimization of injection rates for the conceptual aquifer model from Figures 1 and 3, assuming that structural trapping is the only storage mech-

anism. Using the greedy approach, we start by adding a single well to the largest trapping tree, which consists of six structural traps; see Figure 1. Remember that it is advantageous to place the injection well as deep as possible in the formation to maximize structural trapping. At the same time, we should stay somewhat away from the aquifer boundary. A natural well position is therefore to place the well close to the intersection of the catchment areas of the three deepest traps, so that the injected CO_2 potentially can migrate into three different traps. Figure 5 shows the well position and optimized injection rates that maximizes the objective function (1) over three different time horizons: 500 years, 3000 years, and infinite time. The initial injection rate is set to 0.112 Mt/year so that we inject an amount of CO_2 corresponding to the available pore volume of the four traps in the western part of the trapping tree in ten years. Obviously, we should also be able to fill some of the structural volume of the eastern branch of the trapping tree. With a 500 year time horizon, the optimization algorithm therefore correctly suggests a significantly larger injection rate of 0.216 Mt/year. This time horizon is unfortunately not sufficient to capture the long-term migration of CO_2 toward the aquifer boundary. Indeed, if we increase the horizon on which we measure leakage to 3000 years, we see that the algorithm reduces the injection rates to 0.178 Mt/year. If we instead set an infinite time horizon and use our forecasting method, the optimal injection rate is reduced to 0.163 Mt/year.

Let us also investigate the performance of our forecast algorithm in a little more detail. During an optimization loop, the well rates can (at least in principle) move around in large parts of parameter space and it is important that we have a robust algorithm that manages to capture the correct behavior also when we are quite far from feasible well settings. An important question is: for how long do we need to simulate the VE model before we can invoke the infinite-time forecast? Figure 6 shows three such simulations. With a low injection rate, the only leakage comes from volumes of CO_2 that have been pushed into the catchment region of the boundary during injection. Hence, it is sufficient to only simulate the injection period. If we double the rate, a conservative and reasonably accurate forecast can still be obtained at the time the injection ceases, but the VE simulation should be continued up to 750–800 years to really get a converged forecast. When the rate is doubled one more time, the plume will have so high momentum that it continues to be pushed outward for a time after injection ceases and the VE simulation must be performed up to approximately 300 years before we get an accurate estimate. Since the forecast is inexpensive to compute and its curve basically increases monotonically with time, one can easily formulate an adaptive algorithm that computes a forecast at the end of each time step in the VE simulator and terminate the simulation when this forecast has converged within some prescribed tolerance. (The only technical challenge is to ensure that the resulting state can be used to correctly initiate the adjoint simulation required by the optimization method.)

If we also include residual trapping, the main challenge in providing a forecast at time infinity is to estimate the residual trapping in areas swept by the migrating plume. Unless the plume has a very high momentum and the top surface is planar, the migrating CO_2 will tend to be confined to relatively narrow paths that follow ridges along the top of the aquifer and associated residual trapping will be small. This means that a good forecast can be obtained by only extending the VE simulation to a few years beyond the injection period; this is illustrated in Figure 7, which shows a simulation where we have injected four times the volume of the traps upslope of the injection point. (Notice that this volume is smaller now, compared with Figure 6, because the trapping capacity is also smaller due the residual brine that occupies some of the pore space inside the structural traps.)

4.2 Northern parts of the Utsira formation

We have chosen to study the northern parts of the Utsira formation since here the majority of the trap trees spill in the same direction (i.e., towards the west). Seven wells were placed using the greedy algorithm (see Figure 8), while maintaining a buffer distance of ten kilometers from the formation boundary. An injection period of 50 years was assumed. Fluid parameters used were as per those given by Andersen et al. [1] (however we assumed a sea depth of 100 meters), and rock permeability and porosity used were as per those given by Halland et al. [23]. The results presented in the following are merely intended as illustrations of our computational workflow based on plausible aquifer and fluid properties and storage potentials, well placements, etc., and should not be considered as real operational recommendations.

Using these initial rates gives a scenario in which the migration of CO_2 will continue to be pressure-driven for several years after injection ends before the pressure has dissipated sufficiently so that the system becomes gravity-driven. Our forecast algorithm only looks at how much CO_2 is in a catchment region at a given time, and spills the CO_2 mass from one catchment into another according to how the catchments are connected

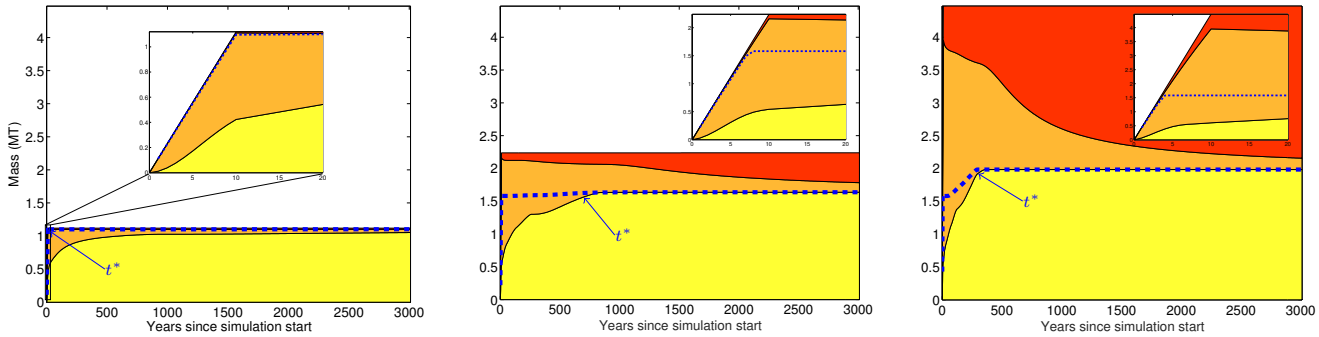

Fig. 6 Forecast of carbon inventory at infinite time for three different rates: initial rate (left), twice the initial rate (middle), and four times the initial rate (right). Here, t^* denotes the minimum end time required for the VE simulation to ensure an accurate forecast of the carbon inventory at time infinity.

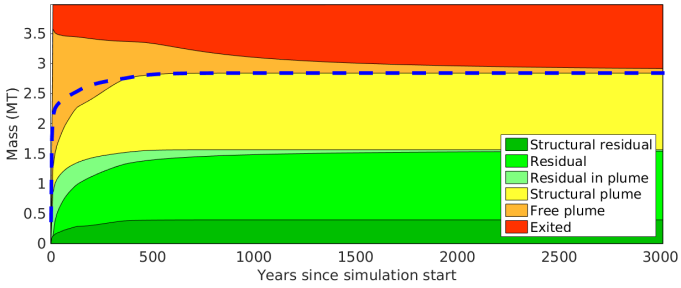

Fig. 7 Forecast at infinite time for the conceptual aquifer model with residual trapping included. The injection rate is four times the initial rate suggested by the greedy well-placement algorithm.

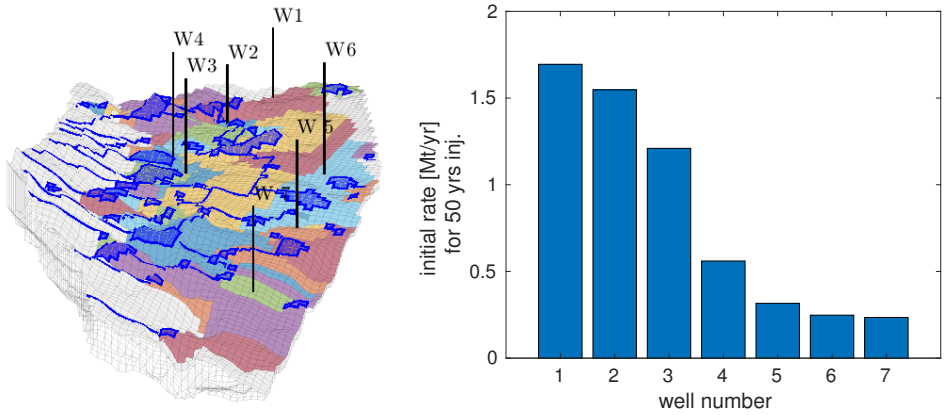

Fig. 8 Northward view of the northern part of the Utsira formation with seven wells placed at the base of spill-paths that spill towards the west of the formation (left). The right plot shows the rates suggested so that a mass equal to the upslope trap capacity is injected in 50 years.

Table 1 Mass inventory for Utsira North during years immediately following a 10-year injection period. Total injected mass by year 10 is 84.738 Mt. Inventory is given in units Mt and percentage of total injected mass, respectively.

Region	**year 10**		**year 20**		**year 30**		**year 40**		**year 50**	
Within trees	84.029	99.16%	83.726	98.81%	83.665	98.73%	83.658	98.73%	83.664	98.73%
- region 37	1.488	1.76%	2.026	2.39%	2.165	2.56%	2.222	2.62%	2.261	2.67%
- region 45	0.041	0.05%	0.043	0.05%	0.043	0.05%	0.043	0.05%	0.043	0.05%
- region 48	82.384	97.22%	81.511	96.19%	81.309	95.95%	81.247	95.88%	81.216	95.84%
- region 53	0.112	0.13%	0.140	0.17%	0.141	0.17%	0.139	0.16%	0.137	0.16%
- region 52	0.003	0.00%	0.004	0.01%	0.005	0.01%	0.005	0.01%	0.005	0.01%
Outside trees	0.633	0.75%	0.823	0.97%	0.843	1.00%	0.829	0.98%	0.807	0.95%

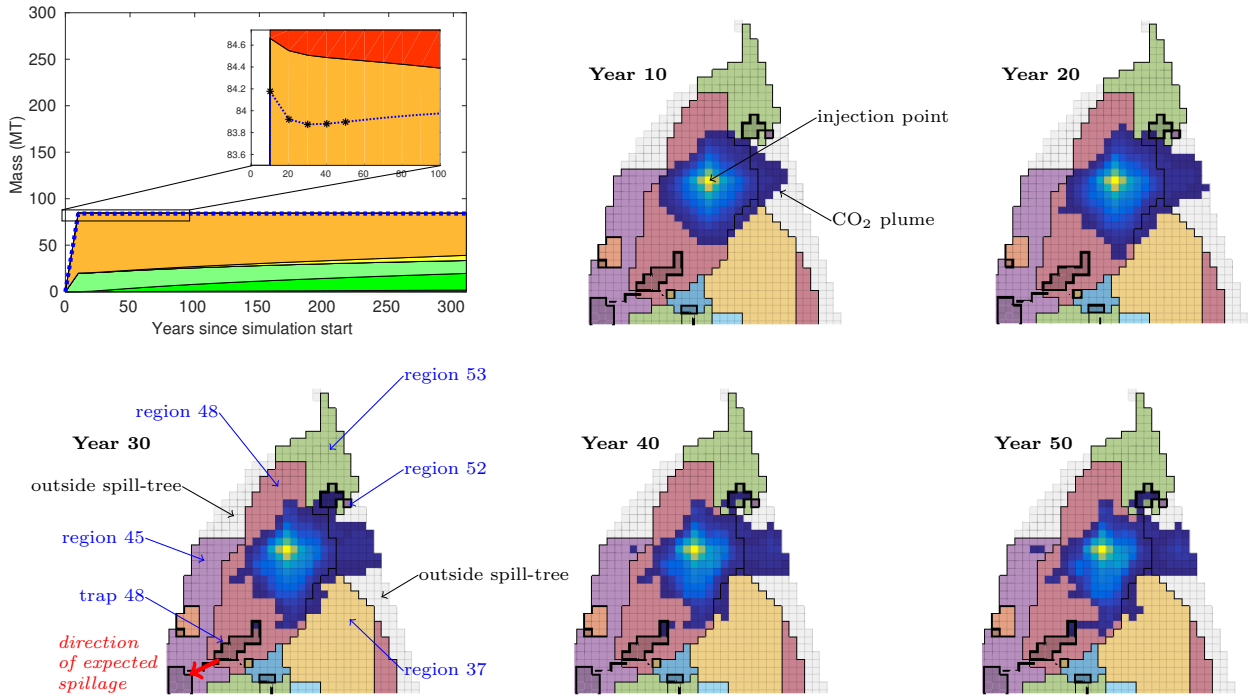

Fig. 9 Simulation of north parts of Utsira where forecast curve exhibits non-monotonic behavior immediately following the injection period. *Upper left:* Trapping inventory with forecast curve in dashed-blue line. *Year 10–50:* Snap-shots of CO_2 saturations around one injection well. High to low CO_2 saturation is indicated by yellow to blue colors, respectively.

along a spill-path. This *gravity-driven spillage* is assumed to occur along each spill-path uniquely, that is, we do not forecast CO_2 spilling from the catchment region of one spill-path to a catchment region of the boundary or a different spill-path; indeed it is not physically expected to do so if it is purely gravity-driven. Yet, it takes some time before the flow becomes purely gravity-driven, and during this time the sweep of the CO_2 continues to extend approximately radially from the injection point, forcing some CO_2 out of one spill-path and into an adjacent spill-path or outside the spill-trees. This *pressure-driven spillage* results in a non-monotone forecast curve.

To highlight this effect, we consider a somewhat simpler case in which only Well 1 was allowed to inject to avoid the impact of other wells. Also, we consider an injection period of 10 years instead of 50, which means Well 1 will operate at a rate of 8.47 Mt/yr instead of 1.69 Mt/yr to exploit the upslope trap capacity of 84.738 Mt. As seen in Figure 9, the forecast curve unexpectedly dips down after year 10, before it begins to converge monotonically (as expected) around year 30 or 40. The inventory in Table 1 explains what is happening. (Note that Well 1 injects directly into region 48 and this mass is expected to fill trap 48 before spilling over into region 45. Also note regions 37, 53, and 52 belong to other spill-trees). Between year 10 and 40, mass is unexpectedly crossing over the boundary from region 48 and into regions 37, 53, 52, and even outside the spill-trees. That is, region 48 contains 82.384 Mt in year 10 and then loses mass by year 20, while regions 37, 53, 52, and the region outside of the spill-trees have all gained mass between year 10 and 20. (We note that region 45 has also gained in mass however this spillage does not conflict with the forecast.) The same thing happens between year 20 and 30: the mass in region 48 decreases while the surrounding regions not belonging to region 48's spill-tree have gained in mass. Until no more mass crosses these boundaries, the forecast curve will not be able to adequately predict the final amount of mass trapped (or mass leaked), and thus the VE simulation must be continued somewhat longer than for the conceptual aquifer model we discussed in Section 4.1.

Coming back to the optimization case with an injection period of 50 years, Figure 10 shows optimized rates of the seven wells obtained by penalizing future leakage. The figure also shows trapping inventory and evolution of the injected CO_2 volumes. It is not surprising that all well rates were increased, given that the wells were placed within a distance of 10 kilometers from the boundary edge so that none of the well's initial rates lead to a CO_2 plume radius that surpassed

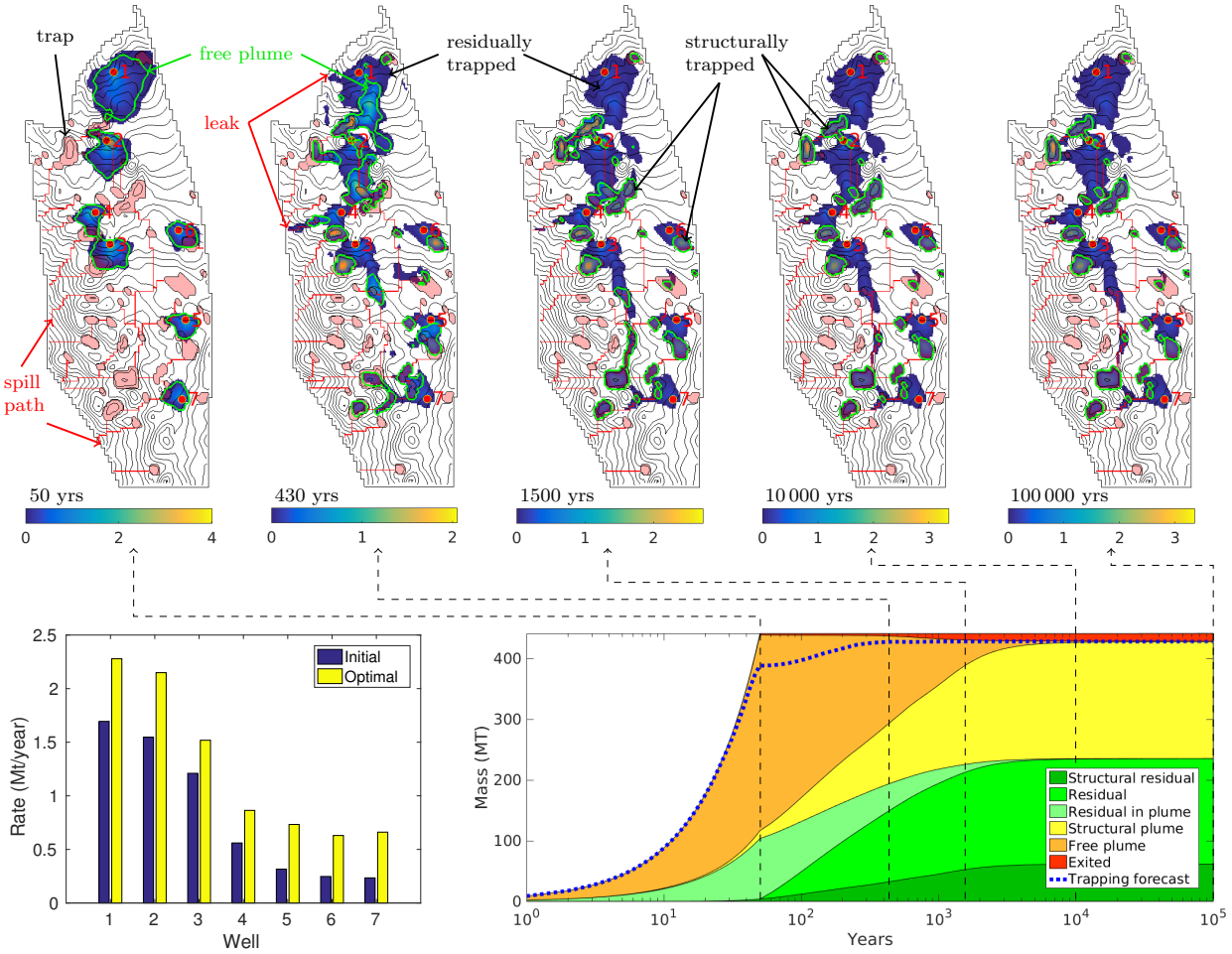

Fig. 10 Optimized injection scenario obtained by penalizing future leakage in Utsira North with leak penalty factor $C = 5$ in (1). Color bar used in snapshots of plume evolution refers to tons of CO_2 per lateral square meter.

the well's distance from the formation boundary. If this had been the case, the optimal well rate that avoids excessive leakage of CO_2 out of the formation would have been lower than the initial rate. The additional trapping can be explained in part by CO_2 spilling into adjacent spill-trees during the time the flow is pressure-driven, and in part by residual trapping as the plume migrates through the formation.

For the optimal rates, the forecast converged approximately 430 years after the start of injection, predicting that 428 Mt of CO_2 would remain in the formation, and by approximately 1000 years the system is essentially driven by buoyancy forces only. The long-term trapping inventory confirms that barely any more leakage occurs after approximately 1500 years of post-injection. By approximately 10,000 years, the free plume has practically been reduced to zero because CO_2 became trapped either structurally or residually as it migrated along the spill-paths. Between year 10,000 and 100,000, there is essentially no change in the flow system.

5 Optimized Utilization within Pressure Limitations

Pressure buildup was not an issue in the previous example since the wells were operating at low enough rates that the induced pressure in the formation could dissipate over the open boundaries and stay well below the overburden pressure of the caprock. As an example of a scenario where pressure buildup may be the main factor limiting the injection, we consider the Bjarmeland formation located in the Barents Sea, which contains a few rather large structural traps. As in the previous section, we assume that the formation has open boundaries modeled using hydrostatic pressure conditions. We emphasize that all results presented in the following are for illustration purposes only and should not be consid-

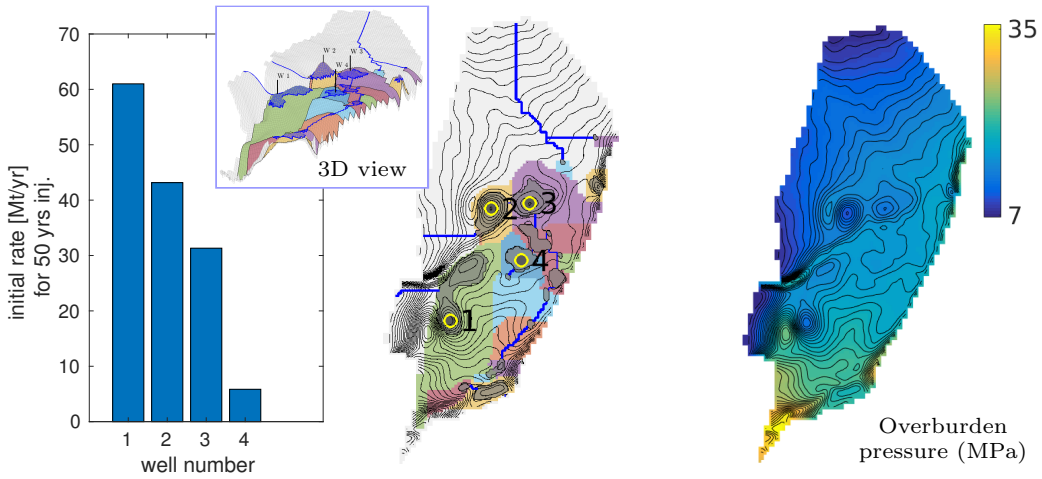

Fig. 11 Setup of a possible injection strategy in the Bjarmeland formation. *Left*: Initial rates of wells that are drilled through the peaks of the four traps with highest structural capacity. *Right*: Overburden pressure of the top surface, calculated by (5).

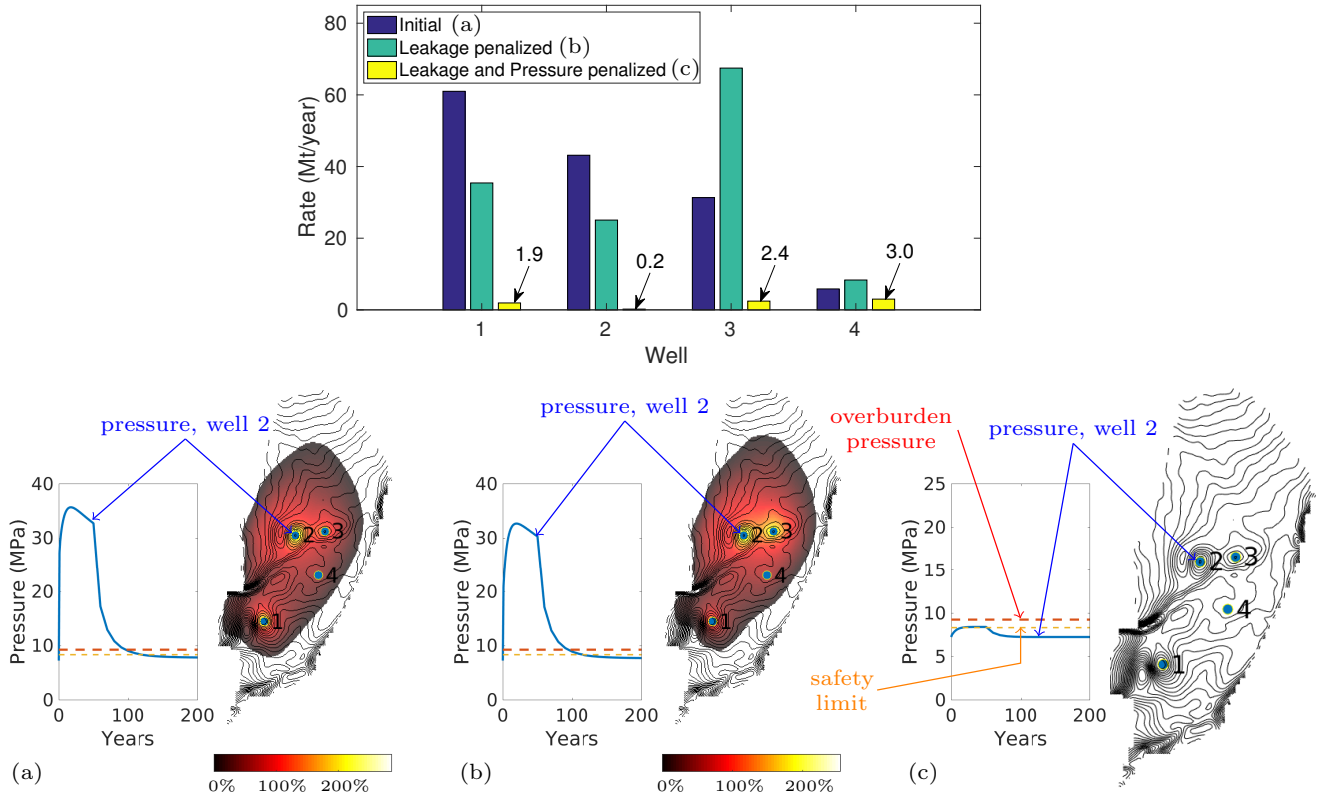

Fig. 12 Comparison of injection rates (upper plot) and pressure buildup (lower plots) under three different injection scenarios for the Bjarmeland formation. From lower left to lower right: initial scenario utilizing storage capacity of the four largest traps, scenario optimized with respect to leakage, and scenario optimized with respect to leakage and pressure buildup. Red to white colors show the pressure violation in terms of how many percent the maximum pressure (out of the entire simulation period) exceeds the overburden pressure, which is shown in Fig. 11.

ered as reliable capacity estimates for the Bjarmeland formation.

When wells are drilled through the peak of the four traps with highest structural capacity, the total mass of 7.07 Gt required to fully exploit the capacity of these traps equate to very high injection rates (see Figure 11). If wells are allowed to operate at these high rates, 812 Mt or 11.5% of the injected mass is forecast to leak and the pressure in the formation increases to 386% of the overburden pressure close to Well 2 (i.e., exceeds the overburden pressure by 286%, see Figure 12). Penalizing leakage using (1) with $C = 5$ suggests a storage plan in which we inject 6.8 Gt, out of which 539 Mt (7.9%) are forecast to eventually leak, however the pressure increases to 354% of the overburden pressure close to Well 2 (i.e., exceeds the overburden pressure by 254%). To maintain the caprock's integrity, we cannot exceed the overburden pressure. Instead we must seek an optimal solution for which both leakage and excess pressure buildup is penalized, i.e., we use (2) rather than (1) as our objective function. We set the pressure limit to be 90% of the overburden pressure, i.e.,

$$p^{\max} = 0.9 \times \left(p_s + \int (\phi \rho_f + (1-\phi)\rho_s) g_z dz \right), \qquad (5)$$

where ρ_f and ρ_s are the fluid and solid densities respectively, ϕ is porosity, and p_s is surface pressure; see Nordbotten et al. [41] for details. The integral is taken vertically over the layers that exist between the surface and the depth of injection; this includes a layer of sea water, and a layer of geological media between the sea bottom and top of the Bjarmeland formation. We assume a surface pressure of 1 atmosphere, and a sea water density of 1000 kg/m^3. The media above the formation is assumed to be comprised of the same type of fluid and rock as in the formation, and so we set this layer's porosity equal to the average of the formation porosity, and the fluid density equal to the formation's initial fluid density. In the overlying layer of media, we assume a rock density of 2000 kg/m^3, as a conservative dry bulk density of sandstone. Thus by using (2) with the given well placement and an injection period of 50 years, the practical amount of CO_2 that could be injected into this formation without compromising the caprock integrity was found to be 0.380 Gt. The most restrictive pressure buildup occurs near Well 2, where the pressure reaches $p^{\max}$. Unlike the two other injection plans, this scenario does not give any leakage, which suggests that this particular formation (with this particular type of well placement) is limited by pressure buildup and not CO_2 leakage.

Of course, it is likely that the Bjarmeland formation could safely and effectively store more CO_2 than what our relatively simple analysis suggests should the wells be placed in different locations, such as farther downslope from the structural traps where the overburden pressure is higher than at the peak of the traps. Or, production wells could be used to extract brine from the formation and to thus manage the pressure buildup. We test out these two possible *pressure management* strategies below. Additionally, a longer injection period could reduce the extent of the CO_2 plume around the wells, thus reducing the amount of mass that spills out from the catchment areas and then leaks from the formation. As the injection period becomes longer, it is possible that the well rates would at some point become limited by leakage rather than pressure buildup.

Pressure Management Strategy 1: By placing the wells farther downslope in the catchment regions of the four largest structural traps, we would likely find higher optimal injection rates due to two reasons: (i) more CO_2 would be trapped as the plume migrates upslope towards the structural trap, and (ii) the overburden pressure is higher at these downslope elevations and thus the pressure limit is less restrictive. We test this out by relocating the four wells to their new positions (see Figure 13a), and obtain their optimal rates using (2). As expected, the optimal rates are higher (see Figure 13b) and more residual trapping has occurred (see trapping inventories in Figure 13d). Figure 13c shows that pressure remains under its limit of 90% (plus a convergence tolerance of 2%) of the overburden pressure across the entire top surface. The largest fraction of the overburden pressure reached occurred near Wells 1, 3, and 4, thus these injection rates can be considered as pressure-limited. We can also consider the injection rate of Well 2 to be pressure-limited even though the pressure profile does not quite reach its limit of ≈14 MPa because of the following: the CO_2 that was injected through Well 2 quickly migrated into the structural trap upslope from the well, and the objective function penalized the pressure at the peak of the trap to keep it within a limit of ≈ 8.5 MPa. This helps to show that our objective function not only penalizes pressure buildup surrounding the wells, but will penalize *any* location in the formation where pressure approaches its predefined limit.

Pressure Management Strategy 2: Back to our original well placement, we add two production wells within an appropriate distance to the injecting wells (i.e., close enough that we adequately manage the pressure near the injection wells but not too close that we provide a leakage path for the migrating CO_2). We optimize the bottom-hole pressure of these production wells in addition to the rates of the injection wells. The bottom-hole pressure of the producers are given a lower limit

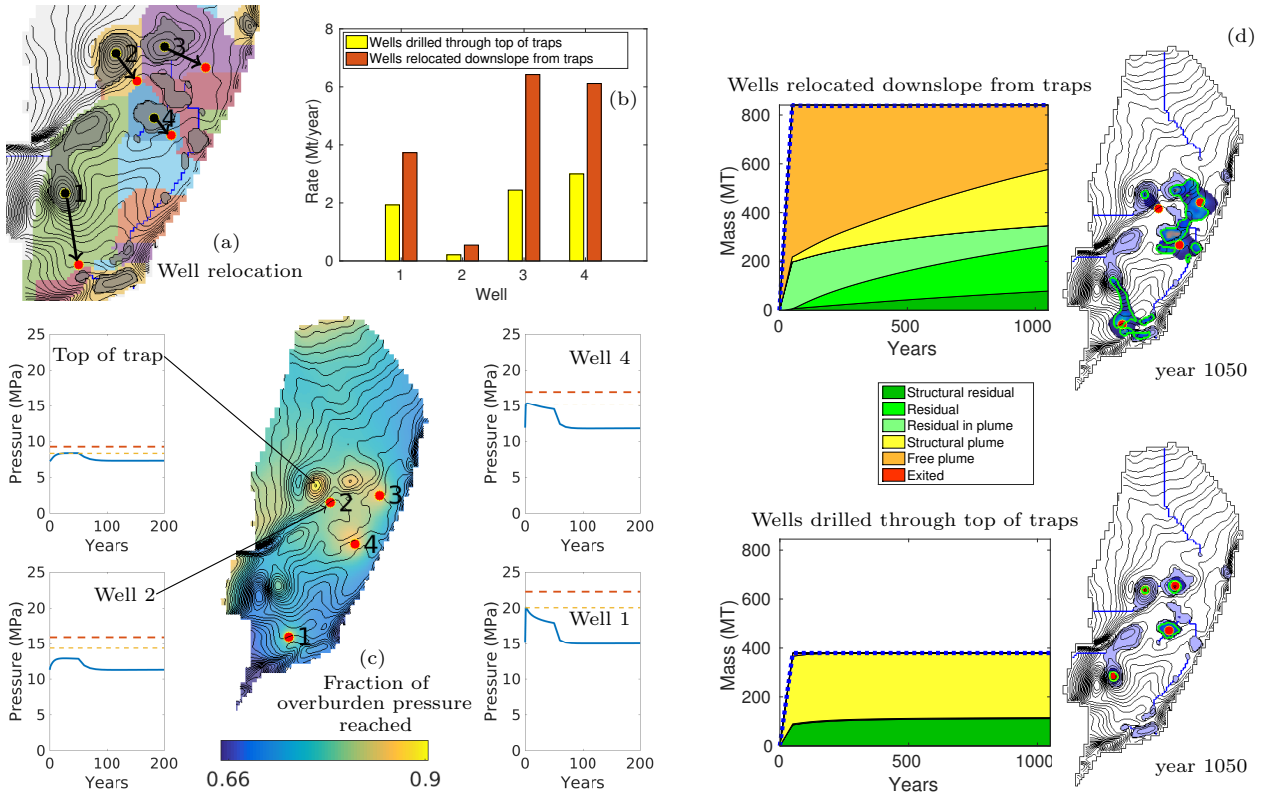

Fig. 13 Pressure management strategy 1: well relocation. (a) Wells are relocated downslope of structural traps, and (b) new optimal rates are obtained while penalizing leakage and pressure buildup. (c) Pressure remains under 90% of the overburden pressure plus a tolerance of 2%, and this limit is reached at the top of the trap nearby Well 2 and at Well 1, 3, and 4. (d) The trapping inventories and saturation profiles show that more residual trapping occurs and the extent of the CO_2 plumes are larger when wells are placed farther downslope.

of 50 bars and an uppper limit of the well cell's initial pressure, which is 103 and 122 bars for Well 5 and 6, respectively. Optimized results are shown in Figure 14. The "optimal" bottom-hole pressures at which to operate Wells 5 and 6 during the injection period end up at the lower limit of 50 bars, which corresponds to a total production of 3.03×10^8 m^3 of water. Extracting the formation fluid allows the injection rates to be higher without compromising the integrity of the caprock, and the optimal amount of CO_2 to inject is increased from 0.380 to 0.574 Gt. The use of production wells is likely to be the most appropriate strategy for managing the pressure buildup in a closed aquifer system.

6 Optimized Utilization within Economic Constraints

We have previously shown our capability to obtain the optimal injection rates such that pressure buildup and/or leakage is limited, however without accounting for the cost of drilling or operating the wells. In this example, we consider injection and storage of CO_2 in the Skade formation, located in the Norwegian North Sea. The model parameters as well as fluid and rock properties that were used for Skade are similar to those for Utsira in Section 4. To interpret the mass of stored CO_2 as a monetary value, we use (3) with a cost $C^{inv} = 5 \cdot 10^6$ USD to drill each well (an assumed value), a combined marginal cost including CO_2 acquisition and well operation of $R^{op} = 50$ USD/tonne (which is within the range of 40–60 USD/tonne reported by Ghomian et al. [21] and Jahangiri and Zhang [26]), and a tax credit rate of $R^{tax} = 51$ USD/tonne (as it was the Norwegian carbon taxation on gasoline in 1999 [10]). We emphasize that these numbers are guesstimates that have been made to illustrate our algorithm. In particular, drilling costs are most likely too low and if CO_2 storage is to become economically viable, tax credit rates need to be (significantly) increased.

Wells are placed using the greedy algorithm, while maintaining buffer distances of 2, 5, and 10 kilometers from adjacent catchment regions, boundary catchment regions, and the formation boundary, respectively. A total of nine wells were placed until the capacity of the next available spill-path was less than 1% of the largest spill-path. The location of the wells in the Skade for-

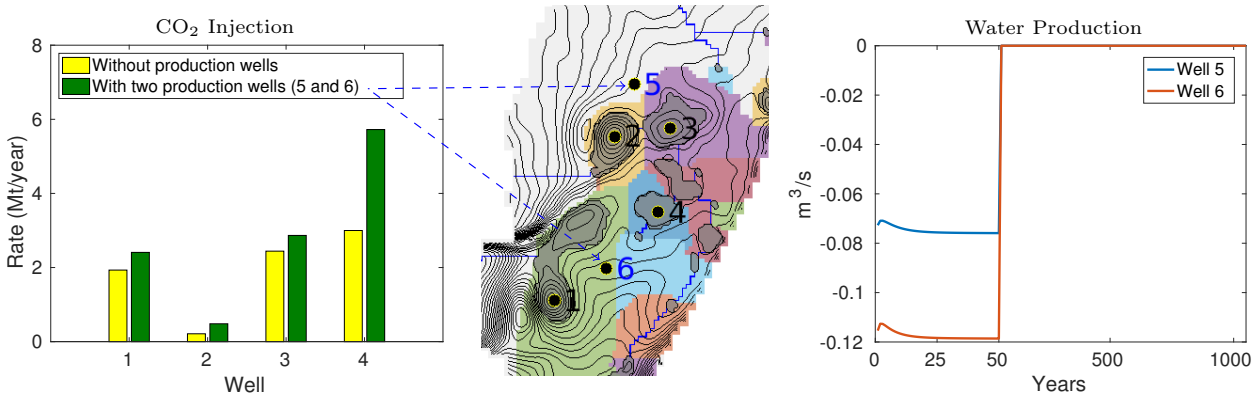

Fig. 14 Pressure management strategy 2: brine extraction. The dynamic storage estimate has been increased from 0.380 to 0.574 Gt when two water producing wells are included.

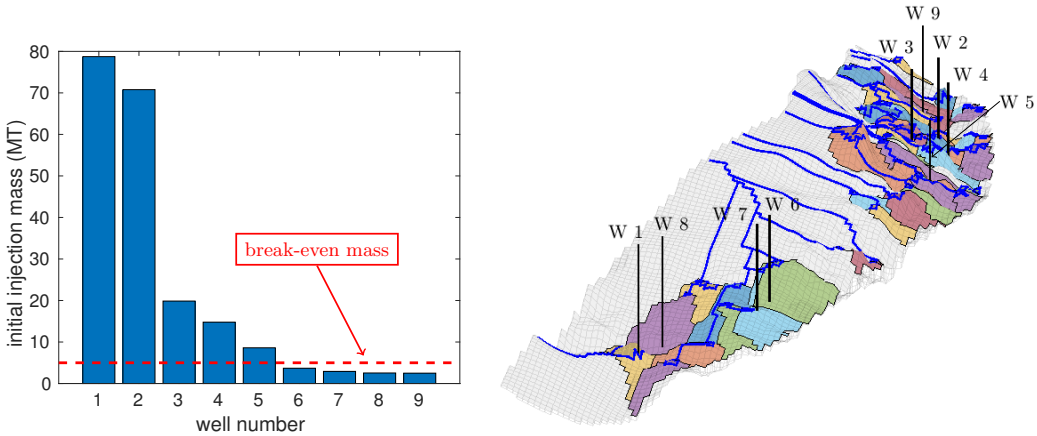

Fig. 15 Well placement (right) and initial masses to inject (left). Rates are simply the initial masses divided by the injection period. The critical (or break-even) mass M_{crit} calculated by (4) is shown by the red-dashed line.

mation and the initial mass to inject per well is shown in Figure 15.

The economic incentive of drilling and operating Wells 6–9 is poor, as their assigned initial rates are lower than the critical rate calculated by (4). Instead of eliminating these wells directly, we screen the economic value of each well using a simulation in which each well individually injects the critical mass. It may happen that more CO_2 than expected can become trapped via other trapping mechanisms (i.e., spilling over into an adjacent spill-path and becoming structurally trapped, or becoming residually trapped as the plume migrates), and this additional amount may be enough to make the well profitable. Moreover, even though Wells 1–5 appear to be economically profitable, we also perform similar simulations to check if enough CO_2 remains trapped in the formation to cover the cost of these wells. Screening results are shown in Table 2, where the total savings were computed by (3). As expected, Wells 6–9 are unable to cover their own costs when injecting the critical amount. Additionally, there is no economic incentive for drilling Well 5, even though there is enough structural capacity in the vicinity of this well to store the critical mass and make the well profitable. However, with an injection period of ten years, 1.8% of the injected mass leaks. In principle, we might be able to store the critical mass without leakage if we extend the injection period (i.e., lower the injection rate), but after trying an injection period of 50 years, we still observed leakage and the well is therefore interpreted as being non profitable.

Thus, we consider Wells 1 to 4 to be the only profitable wells and optimize their rates using (3) with a leakage penalty factor of ten ($C = 10$) in order to associate a cost for the leaked CO_2 in addition to the cost of its injection. For comparison, we also obtain the optimal rates when the other wells were included to highlight that Wells 5 to 9 do not add value to the injection schedule. We also investigate whether or not all of the first four wells are required to obtain the maximum savings. For example, if the value of trapped CO_2 injected by Well 3 were to equal the combined value offered by Wells 3 and 4, then there would be no real incentive to drilling and operating Well 4.

Table 2 Wells that can and cannot pay for themselves when individually injecting the critical mass M_{crit} over an injection period of ten years. Masses are in megatonnes and savings (or deficit) in millions USD computed by (3) with a leakage penalty factor of $C = 1$.

Well	1	2	3	4	5	6	7	8	9
Stored mass [Mt]	5.0	5.0	5.0	5.0	4.91	4.13	4.93	4.52	4.91
Leaked mass [Mt]	—	—	—	—	0.09	0.87	0.07	0.48	0.09
	—	—	—	—	1.8%	17.3%	1.5%	9.6%	1.8%
Deficit [mill USD]	—	—	—	—	-4.5	-44.1	-3.7	-24.5	-4.5

Table 3 Comparison of optimized savings in million USD (obtained using (3) with $C = 10$) and return of investment for different well combinations in the Skade formation. Return of investment is defined as savings divided by the sum of drilling and operation costs. We emphasize that the numbers reported are only intended as illustrations of a computational workflow and should not be interpreted as being representative for a real storage scenario in the Skade formation.

Wells	Value injected	Leakage cost	Drilling cost	Operation cost	Savings / return	
1	1489.6801	-4.9387	-5.0000	-1460.4706	19.324	1.32%
1 to 2	5294.2213	-17.7287	-10.0000	-5190.4130	76.187	1.47%
1 to 3	6462.9556	-21.4410	-15.0000	-6336.2310	90.444	1.42%
1 to 4	6971.0345	-13.9936	-20.0000	-6834.3476	102.908	1.50%
1 to 5	7071.0166	-14.3025	-25.0000	-6932.3692	99.613	1.43%
1 to 6	7171.4692	-94.1861	-30.0000	-7030.8521	16.752	0.24%
1 to 7	7277.0532	-95.9491	-35.0000	-7134.3658	12.113	0.17%
1 to 8	6897.6821	-97.0304	-40.0000	-6762.4334	-1.353	-0.02%
1 to 9	7032.1874	-100.1946	-45.0000	-6894.3014	-6.826	-0.10%

Table 3 summarizes the results of our analysis, and here we see that maximum savings are indeed made when the first four wells are used together; a savings of 102.9 million USD is achieved. In comparison, use of Wells 1 to 3 yields a savings of 90.4 million USD, Wells 1 to 5 yields a savings of 99.6 million USD, and if all nine wells were drilled and operated, a deficit of -6.8 million USD occurs. The fact that drilling and operating Wells 1 to 5 cannot yield a savings greater than what is possible with only the first four wells confirms what we determined during the screening stage, i.e., Well 5 is not a worthwhile investment. This is also highlighted by the fact that the optimized rate of Well 5 is below the critical rate required for a well to be profitable (see Figure 16).

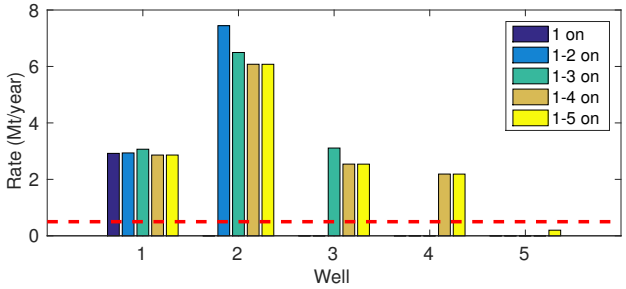

Fig. 16 Optimal rates for the Skade formation obtained while penalizing leakage and accounting for well costs. Maximum savings is achieved when Wells 1 to 4 are drilled and operated (see Table 3).

7 Optimization details

We briefly compare some numerical quantities for the first two large-scale optimization problems solved in this study; see Table 4. All cases were run on a workstation with an Intel Xeon E5-2640 v3 processor and 64 GB of memory. The time it takes to perform one forward simulation is influenced by the number of grid cells, number of time steps, and the number of well controls (as well as their rates). The Utsira North model is comprised of 4748 cells and has seven injectors, whereas the Bjarmeland model has 7832 cells, four injectors, and either zero or two producers. Both examples use 50 steps for an injection period of 50 years, and 100 steps for the migration period of 1000 years. The number of simulations required to reach the optimal solution depends on several factors such as the convergence tolerance and initial guess. That is, the optimization is considered converged when the objective value changes less than 10^{-3} times the objective value of the initial simulation. We also limit the number of iterations in each line search to five.

As shown in Table 4, some of the Bjarmeland cases require many simulations and take a very long time to converge to the optimal solution. These long run times are likely caused by the need to iterate through five or six optimization loops, where the pressure penalty factor C_p is gradually ramped up. Case (iv) does not require as many simulations as (ii) or (iii), primarily because we use the optimized rates from case (ii) as a very good initial guess.

Table 4 Comparison of optimization run times and other numerical quantities. '-' denotes C_p loops not required.

Example	# wells	CPU time	total # simulations	total # line searches	# C_p loops
Utsira North					
penalize leakage	7	0h 32min	24	6	-
Bjarmeland					
(i) penalize leakage	4	1h 38min	29	7	-
(ii) penalize leakage and pressure	4	6h 19min	177	49	5
(iii) well relocation	4	8h 24min	235	68	6
(iv) include production wells	6	2h 59min	74	39	5

We recognize that ramping up the pressure penalty factor C_p is not the most efficient approach, because several optimization loops are required. As alluded to in Section 3.3, an alternative approach would be to *constrain* the pressure to a predefined limit $p_i^{\max}$, rather than *penalize* it with a quadratic pressure term as in (2). Another way to achieve shorter CPU times is to reduce the number of migration years in each forward simulation, in cases where leakage is not expected to be the limiting factor. For the optimization cases (ii)–(iv) in the (open system) Bjarmeland example, the maximum pressure violation always occurs at some point in time during the injection period, and essentially no leakage occurs. As such, there is no need to simulate a thousand years of migration. Also, an initial guess that is based on the upslope trapping capacity is more appropriate in cases where leakage will be the limiting factor rather than pressure buildup. Running the optimization problem on a coarsely resolved grid first could help identify an appropriate initial guess that could be applied to the finely resolved grid. We leave these above mentioned strategies of reducing optimization run times as the subject for future work.

8 Summary and Conclusions

This work shows how one can obtain an ideal injection strategy that utilizes the CO_2 storage capacity of large-scale formations while taking into account various constraints and limitations. The optimization framework used has been explained in previous work, however, here we account for limitations due to the caprock overburden pressure as well as the cost of drilling and operating the wells. Also, we proposed a forecasting algorithm based on spill-point analysis that enabled us to reduce the number of migration years required in our simulations to capture the ultimate amount of CO_2 bound to leak from the formation.

We considered three examples of objective functions: the first (and simplest) penalized the forecast leakage only, the second penalized pressure buildup in addition to leakage, and the third penalized leakage and converted the stored CO_2 into a monetary value in order to account for well costs. We used a synthetic grid made from a sloping and undulating top surface to demonstrate the capability of our leak forecasting algorithm. Then, we applied this algorithm to the northern part of Utsira, a real formation found along the Norwegian Continental Shelf, to obtain optimal rates of seven placed wells. Using this example, we also explained why our forecast curve may be non-monotone immediately following the injection period before it converges. The second and third objective functions were applied to the Bjarmeland and Skade formations, respectively, and we considered the use of production wells for pressure management in Bjarmeland.

Using data from real formations on the Norwegian Continental Shelf, we demonstrated how fast algorithms implemented in MRST can be used to investigate various injection plans and scenarios related to CO_2 storage. We obtained results that were visually intuitive and helped to provide *dynamic* storage capacity estimates of real formations. However, the estimates we have reported for Utsira, Bjarmeland, and Skade are not intended to be used in developing real CO_2 storage plans for the following reasons: several parameters have been assumed (i.e., cost to drill and operate wells, the safety factor applied to the overburden pressure, etc.), and the formation datasets are coarsely resolved, contain uniform rock properties, and do not provide fault information. None the less, our simulation and optimization method could still be applied to refined and more accurate datasets to provide better storage capacity estimates if required.

The optimization methods used herein penalized leakage over an infinite time horizon; this avoids making assumptions of what would be a reasonable geological time scale, over which the aquifer geology can be assumed to remain the same. For how long CO_2 should remain in a rock formation to be considered permanently stored is more a political and regulatory question. However, regardless of whether this time is set to be hundreds, thousands, or million of years, our algo-

rithms can be used to optimize the achievable storage capacity under the assumptions of an invariant geological model.

Acknowledgements The work was funded in part by the Research Council of Norway through grant no. 243729 (Simulation and optimization of large-scale, aquifer-wide CO_2 injection in the North Sea).

References

1. Andersen, O., Nilsen, H.M., Lie, K.A.: Reexamining CO2 storage capacity and utilization of the Utsira Formation. In: ECMOR XIV – 14th European Conference on the Mathematics of Oil Recovery, Catania, Sicily, Italy, 8-11 September. EAGE (2014). DOI 10.3997/2214-4609.20141809
2. Bachu, S.: Review of CO2 storage efficiency in deep saline aquifers. Int. J. Greenh. Gas Con. pp. 1–15 (2015). DOI 10.1016/j.ijggc.2015.01.007
3. Bachu, S., Melnik, A., Bistran, R.: Approach to evaluating the CO2 storage capacity in Devonian deep saline aquifers for emissions from oil sands operations in the Athabasca area, Canada. Energy Procedia **63**, 5093–5102 (2014). DOI 10.1016/j.egypro.2014.11.539
4. Bellout, M.C., Echeverría Ciaurri, D., Durlofsky, L.J., Foss, B., Kleppe, J.: Joint optimization of oil well placement and controls. Comput. Geosci. **16**(4), 1061–1079 (2012). DOI 10.1007/s10596-012-9303-5
5. Bentham, M., Mallows, T., Lowndes, J., Green, A.: CO2 STORage Evaluation Database (CO2 Stored). the UK's online storage atlas. Energy Procedia **63**(0), 5103–5113 (2014). DOI 10.1016/j.egypro.2014.11.540
6. Birkholzer, J.T., Oldenburg, C.M., Zhou, Q.: CO2 migration and pressure evolution in deep saline aquifers. Int. J. Greenh. Gas Con. **40**, 203–220 (2015). DOI 10.1016/j.ijggc.2015.03.022
7. Bøe, R., Magnus, C., Osmundsen, P.T., Rindstad, B.I.: CO2 point sources and subsurface storage capacities for CO2 in aquifers in Norway. Tech. rep., Geological Survey of Norway, Trondheim (2002)
8. Bradshaw, B.E., Spencer, L.K., Lahtinen, A.L., Khider, K., Ryan, D.J., Colwell, J.B., Chirinos, A., Bradshaw, J., Draper, J.J., Hodgkinson, J., McKillop, M.: An assessment of Queensland's CO2 geological storage prospectivity–The Queensland CO2 geological storage atlas. Energy Procedia **4**(0), 4583–4590 (2011). DOI 10.1016/j.egypro.2011.02.417
9. Bradshaw, J., Bachu, S., Bonijoly, D., Burruss, R., Holloway, S., Christensen, N.P., Mathiassen, O.M.: CO2 storage capacity estimation: Issues and development of standards. Int. J. Greenh. Gas Con. **1**(1), 62–68 (2007). DOI 10.1016/S1750-5836(07)00027-8
10. Bruvoll, A., Larsen, B.M.: Greenhouse gas emissions in Norway: Do carbon taxes work? Statistics Norway Discussion Papers 337, Statistics Norway, Kongsvinger (2002). http://www.ssb.no
11. Cavanagh, A.J., Haszeldine, R.S., Nazarian, B.: The Sleipner CO2 storage site: using a basin model to understand reservoir simulations of plume dynamics. First Break **33**(June), 61–68 (2015)
12. Chen, C., Li, G., Reynolds, A.: Robust constrained optimization of short- and long-term net present value for closed-loop reservoir management. SPE J. **17**(03), 849–864 (2012). DOI 10.2118/141314-pa
13. Class, H., Ebigbo, A., Helmig, R., Dahle, H.K., Nordbotten, J.M., Celia, M.a., Audigane, P., Darcis, M., Ennis-King, J., Fan, Y., Flemisch, B., Gasda, S.E., Jin, M., Krug, S., Labregere, D., Naderi Beni, A., Pawar, R.J., Sbai, A., Thomas, S.G., Trenty, L., Wei, L.: A benchmark study on problems related to CO2 storage in geologic formations. Comput. Geosci. **13**(4), 409–434 (2009). DOI 10.1007/s10596-009-9146-x
14. Class, H., Kissinger, A., Knopf, S., Konrad, W., Noack, V., Scheer, D.: Combined Natural and Social Science Approach for Regional-Scale Characterisation of CO2 Storage Formations and Brine Migration Risks (CO2BRIM), pp. 209–227. Springer International Publishing, Cham (2015). DOI 10.1007/978-3-319-13930-2_10
15. Cloete, M.: Atlas on geological storage of carbon dioxide in South Africa. Tech. rep., Council for Geoscience, Johannesburg, South Africa (2010). sacccs.org.za/wp-content/uploads/2010/11/Atlas.pdf
16. Craig, J., Gorecki, C.D., Ayash, S.C., Liu, G., Braunberger, J.R.: A comparison of volumetric and dynamic storage efficiency in deep saline reservoirs: An overview of IEAGHG study IEA/CON/13/208. Energy Procedia **63**, 5185–5191 (2014). DOI 10.1016/j.egypro.2014.11.549
17. Eigestad, G.T., Dahle, H.K., Hellevang, B., Riis, F., Johansen, W.T., Øian, E.: Geological modeling and simulation of CO2 injection in the Johansen formation. Comput. Geosci. **13**(4), 435–450 (2009). DOI 10.1007/s10596-009-9153-y
18. Elenius, M.T., Nordbotten, J.M., Kalisch, H.: Convective mixing influenced by the capillary transition zone. Comput. Geosci. **18**(3), 417–431 (2014). DOI 10.1007/s10596-014-9415-1
19. Estublier, A., Lackner, A.S.: Long-term simulation of the Snøhvit CO2 storage. Energy Procedia **1**(1), 3221–3228 (2009). DOI 10.1016/j.egypro.2009.02.106
20. Gasda, S.E., Nordbotten, J.M., Celia, M.A.: Application of simplified models to CO2 migration and immobilization in large-scale geological systems. Int. J. Greenh. Gas Con. **9**, 72–84 (2012). DOI 10.1016/j.ijggc.2012.03.001
21. Ghomian, Y., Urun, M.B., Pope, G.A., Sepehrnoori, K.: Investigation of economic incentives for CO2 sequestration. In: SPE Annual Technical Conference and Exhibition. Society of Petroleum Engineers (2008). DOI 10.2118/116717-MS
22. Grøver, A., Rinna, J., Lothe, A.E., Bergmo, P., Wessel-Berg, D.: How and when could basin modelling approaches be useful for CO2 storage assessment. In: 7th Trondheim CCS Conference, 4th-5th of June (2013)
23. Halland, E.K., Mujezinović, J., Riis, F. (eds.): CO_2 Storage Atlas: Norwegian Continental Shelf. Norwegian Petroleum Directorate (2014). npd.no/en/Publications/Reports/Compiled-CO2-atlas
24. Hou, J., Zhou, K., Zhang, X.S., Kang, X.D., Xie, H.: A review of closed-loop reservoir management. Pet. Sci. **12**(1), 114–128 (2015). DOI 10.1007/s12182-014-0005-6
25. International Energy Agency: Key World Energy Statistics 2015 (2015). tinyurl.com/zkp2af3
26. Jahangiri, H.R., Zhang, D.: Ensemble based co-optimization of carbon dioxide sequestration and enhanced oil recovery. Int. J. Greenh. Gas Con. **8**, 22–33 (2012). DOI 10.1016/j.ijggc.2012.01.013
27. Jansen, J.D.: Adjoint-based optimization of multi-phase flow through porous media – a review. Computers & Fluids **46**(1), 40–51 (2011). DOI 10.1016/j.compfluid.2010.09.039. 10th {ICFD} Conference Series on Numerical Methods for Fluid Dynamics (ICFD 2010)

28. Krogstad, S., Lie, K.A., Møyner, O., Nilsen, H.M., Raynaud, X., Skaflestad, B.: MRST-AD – an open-source framework for rapid prototyping and evaluation of reservoir simulation problems. In: SPE Reservoir Simulation Symposium, 23–25 February, Houston, Texas (2015). DOI 10.2118/173317-MS
29. Lewis, D., Bentham, M., Cleary, T., Vernon, R., O'Neill, N., Kirk, K., Chadwick, A., Hilditch, D., Michael, K., Allinson, G., Neal, P., Ho, M.: Assessment of the potential for geological storage of carbon dioxide for the island of Ireland. Tech. rep., Sustainable Energy Ireland, Environmental Protection Agency, Geological Survey of Northern Ireland, and Geological Survey of Ireland (2008)
30. Lie, K.A., Krogstad, S., Ligaarden, I.S., Natvig, J.R., Nilsen, H.M., Skaflestad, B.: Open source MATLAB implementation of consistent discretisations on complex grids. Comput. Geosci. **16**(2), 297–322 (2012). DOI 10.1007/s10596-011-9244-4
31. Lie, K.A., Nilsen, H.M., Andersen, O., Møyner, O.: A simulation workflow for large-scale CO2 storage in the Norwegian North Sea. Comput. Geosci. **20**(3), 607–622 (2016). DOI 10.1007/s10596-015-9487-6
32. Lothe, A.E., Emmel, B., Grøver, A., Bergmo, P.E.: CO2 storage modelling and capacity estimation for the Trøndelag platform, offshore Norway - using a basin modelling approach. Energy Procedia **63**(1876), 3648–3657 (2014). DOI 10.1016/j.egypro.2014.11.394
33. MRST: The MATLAB Reservoir Simulation Toolbox. www.sintef.no/MRST (2016a)
34. MRST-co2lab: Numerical CO_2 laboratory. www.sintef.no/co2lab (2016a)
35. Natural Resources Canada, Mexican Ministry of Energy, and U.S. Department of Energy: The North American Carbon Storage Atlas (2012). www.cacsap.org
36. Nilsen, H.M., Lie, K.A., Andersen, O.: Analysis of CO_2 trapping capacities and long-term migration for geological formations in the Norwegian North Sea using MRST-co2lab. Computers & Geosciences **79**, 15–26 (2015). DOI 10.1016/j.cageo.2015.03.001
37. Nilsen, H.M., Lie, K.A., Andersen, O.: Fully-implicit simulation of vertical-equilibrium models with hysteresis and capillary fringe. Comput. Geosci. **20**(1), 49–67 (2016). DOI 10.1007/s10596-015-9547-y
38. Nilsen, H.M., Lie, K.A., Andersen, O.: Robust simulation of sharp-interface models for fast estimation of CO2 trapping capacity. Comput. Geosci. **20**(1), 93–113 (2016). DOI 10.1007/s10596-015-9549-9
39. Nilsen, H.M., Lie, K.A., Møyner, O., Andersen, O.: Spill-point analysis and structural trapping capacity in saline aquifers using MRST-co2lab. Computers & Geosciences **75**, 33–43 (2015). DOI 10.1016/j.cageo.2014.11.002
40. Nilsen, H.M., Syversveen, A.R., Lie, K.A., Tveranger, J., Nordbotten, J.M.: Impact of top-surface morphology on CO2 storage capacity. Int. J. Greenh. Gas Control **11**(0), 221–235 (2012). DOI 10.1016/j.ijggc.2012.08.012
41. Nordbotten, J.M., Celia, M.A.: Geological Storage of CO2: Modeling Approaches for Large-Scale Simulation. John Wiley & Sons, Inc. (2012)
42. Nordbotten, J.M., Flemisch, B., Gasda, S.E., Nilsen, H.M., Fan, Y., Pickup, G.E., Wiese, B., Celia, M.A., Dahle, H.K., Eigestad, G.T., Pruess, K.: Uncertainties in practical simulation of CO2 storage. Int. J. Greenh. Gas Control **9**(0), 234–242 (2012). DOI 10.1016/j.ijggc.2012.03.007
43. Pachauri, R.K., Allen, M.R., Barros, V.R., Broome, J., Cramer, W., Christ, R., Church, J.A., Clarke, L., Dahe, Q., Dasgupta, P., othersa: Climate Change 2014: Synthesis Report. Contribution of Working Groups I, II and III to the Fifth Assessment Report of the Intergovernmental Panel on Climate Change. IPCC, Geneva, Switzerland (2014)
44. Popova, O.H., Small, M.J., McCoy, S.T., Thomas, A.C., Rose, S., Karimi, B., Carter, K., Goodman, A.: Spatial stochastic modeling of sedimentary formations to assess CO2 storage potential. Environ. Sci. Technol. **48**(11), 6247–6255 (2014). DOI 10.1021/es501931r
45. Roerdink, J.B.T.M., Meijster, A.: The watershed transform: Definitions, algorithms and parallelization strategies. Fund. inform. **41**(1, 2), 187–228 (2000). DOI 10.1007/978-3-7091-6867-7_3
46. Sylta, Ø.: Hydrocarbon migration modelling and exploration risk. Ph.D. thesis, Norwegian University of Science and Technology, Faculty of Engineering Science and Technology, Department of Geology and Mineral Resources Engineering (2004)
47. U.S. Department of Energy, Office of Fossil Energy: The 2012 United States Carbon Utilization and Storage Atlas, fourth edn. (2012). netl.doe.gov/research/coal/carbon-storage/atlasiv
48. Watson, F.E., Mathias, S.A., Daniels, S.E., Jones, R.R., Davies, R.J., Hedley, B.J., van Hunen, J.: Dynamic modeling of a UK North Sea saline formation for CO2 sequestration. Petrol. Geosci. **20**(2), 169–185 (2014). DOI 10.1144/petgeo2012-072
49. Wei, L., Saaf, F.: Estimate CO2 storage capacity of the Johansen formation: numerical investigations beyond the benchmarking exercise. Comput. Geosci. **13**(4), 451–467 (2009). DOI 10.1007/s10596-008-9122-x
50. Wolfe, P.: Convergence conditions for ascent methods. SIAM Rev. **11**(2), 226–235 (1969). DOI 10.1137/1011036
51. Wolfe, P.: Convergence conditions for ascent methods. II: Some corrections. SIAM Rev. **13**(2), 185–188 (1971). DOI 10.1137/1013035